PAPER • OPEN ACCESS

The experimental realization of high-fidelity 'shortcut-to-adiabaticity' quantum gates in a superconducting Xmon qubit

To cite this article: Tenghui Wang *et al* 2018 *New J. Phys.* **20** 065003

View the article online for updates and enhancements.

Related content

Recent citations

New Journal of Physics

The open access journal at the forefront of physics

PAPER

The experimental realization of high-fidelity 'shortcut-to-adiabaticity' quantum gates in a superconducting Xmon qubit

Tenghui Wang[1], Zhenxing Zhang[1], Liang Xiang[1], Zhilong Jia[2], Peng Duan[2], Weizhou Cai[3], Zhihao Gong[1], Zhiwen Zong[1], Mengmeng Wu[1], Jianlan Wu[1], Luyan Sun[3], Yi Yin[1] and Guoping Guo[2]

[1] Physics Department, Zhejiang University, Hangzhou, 310027, People's Republic of China
[2] Key Laboratory of Quantum Information, University of Science and Technology of China, Hefei, 230026, People's Republic of China
[3] Center for Quantum Information, Institute for Interdisciplinary Information Sciences, Tsinghua University, Beijing, 100084, People's Republic of China

E-mail: jianlanwu@zju.edu.cn, yiyin@zju.edu.cn and gpguo@ustc.edu.cn

Keywords: quantum gate, shortcut-to-adiabaticity, superconducting qubits

Abstract

Based on a 'shortcut-to-adiabaticity' (STA) scheme, we theoretically design and experimentally realize a set of high-fidelity single-qubit quantum gates in a superconducting Xmon qubit system. Through a precise microwave control, the qubit is driven to follow a fast 'adiabatic' trajectory with the assistance of a counter-diabatic field and the correction of derivative removal by adiabatic gates. The experimental measurements of quantum process tomography and interleaved randomized benchmarking show that the process fidelities of our STA quantum gates are higher than 94.9% and the gate fidelities are higher than 99.8%, very close to the state-of-art gate fidelity of 99.9%. An alternate of high-fidelity quantum gates is successfully achieved under the STA protocol.

1. Introduction

Quantum computation and quantum information processing are programmed through sequential operations of various quantum gates, which are built bottom up from simple but fundamental single- and two-qubit gates [1, 2]. A gate error has to be controlled below a fault-tolerant threshold in scale-up quantum computation. Since this error threshold is usually small (0.1%–1%), the experimental realization of high-fidelity quantum gates is an essential task in various artificial quantum systems such as nuclear magnetic resonance [3, 4], ion traps [5] and superconducting circuits [6].

A unitary transformation occurs when a single- or multi-qubit system is operated by a quantum gate. For a single-qubit, such a unitary transformation can be viewed as a rotation of a qubit vector, which can be mapped onto a spin, on the Bloch sphere. Subject to an external magnetic field along a fixed direction, the rotation angle of the spin is controlled by adjusting the amplitude of the magnetic field over time. By mapping a driving pulse, e.g., Gaussian-shaped, onto a magnetic field, we can build a single-qubit quantum gate based on the above scheme. This standard approach has been applied in almost all the artificial quantum devices. In superconducting qubit systems, the highest single-qubit fidelity is achieved at the level of >99.9% by optimizing the pulse amplitude and frequency [6].

An alternative way of constructing quantum gates is to change the direction of the magnetic field over time. In a special moving reference frame, the motion of the spin can be highly simplified. In a quantum adiabatic operation, the qubit is kept at its instantaneous eigenstates. With respect to the instantaneous eigenbasis, the qubit vector is rotated along a fixed latitude on a moving Bloch sphere by accumulating dynamic and geometric phases [7, 8]. At the end of such an quantum adiabatic operation, an arbitrary quantum gate is realized by the combined effect of a simple spin rotation in the moving frame and the rotation of the reference frame.

However, an ideal adiabatic operation can only be performed with an infinitely slow speed. A practically adiabatic implementation inevitably includes errors due to non-adiabatic transition and quantum dissipation. The associated long operation time leads to a technical difficulty in scale-up quantum computation. The

shortcut-to-adiabaticity (STA) procedure has been proposed to solve these problems by introducing a counter-diabatic field in addition to the reference fast 'adiabatic' field [9–17]. The qubit system is driven to follow the reference 'adiabatic' trajectory by suppressing the non-adiabatic transitions. As the quantum operation is accelerated ten to hundred times, the decoherence induced error can be significantly reduced. The STA protocol has been well implemented experimentally soon after it was proposed theoretically [18–22]. In our recent experiments with a superconducting phase qubit, we successfully measured the Berry phase [23] and achieved a high-fidelity state transfer under the STA protocol [24]. The state transfer technique was further applied to simulate a quantum topological phase transition [24].

In this paper, we extend our previous work of quantum state transfer for the purpose of single-qubit STA quantum gates. Our theoretical design shares the same principle as in a recent proposal in the system of NV centers [25]. The detailed driving pulse is different but preserves the utilization of the phase accumulation in the fast 'adiabatic' evolution. The STA gate operations are also discussed in recent theoretical proposals [26, 27]. With the improvement from a superconducting phase to Xmon qubit, the high-fidelity STA quantum gate is successfully achieved, as demonstrated by our quantum process tomography (QPT) and interleaved randomized benchmarking measurements. For our examples of the rotations about X-, Y- and Z-axes and the Hadamard gate, the gate fidelity is consistently higher than 99.8%, which promises an alternative choice of quantum gates for a practical application.

2. Theory

In this section, we demonstrate our theoretical design of a general single-qubit gate performed under the 'shortcut-to-adiabaticity' (STA) protocol.

2.1. Adiabatic quantum gate
A single-qubit of $\{|0\rangle, |1\rangle\}$ can be mapped onto a spin-1/2 particle $\{|\uparrow\rangle, |\downarrow\rangle\}$ driven by an external field [1]. In the rotating frame, the time-dependent Hamiltonian is written as

$$H_0(t) = \hbar B_0(t) \cdot \boldsymbol{\sigma}/2, \tag{1}$$

where $B_0(t) = \Omega(t)(\sin\theta(t)\cos\phi(t), \sin\theta(t)\sin\phi(t), \cos\theta(t))$ is the vector of an external field and $\boldsymbol{\sigma} = (\sigma_x, \sigma_y, \sigma_z)$ is the vector of Pauli matrices. The amplitude $\Omega(t)$, the polar angle $\theta(t)$ and the azimuthal angle $\phi(t)$ are modulated by microwave pulse sequences in our experiment [23, 24]. At a given time t, the instantaneous eigenstates, $\{|\psi_+(t)\rangle, |\psi_-(t)\rangle\}$, are obtained by a rotation of the reference states, $\{|\uparrow\rangle, |\downarrow\rangle\}$, where the rotation matrix to change the frame is given by

$$S(t) = \begin{pmatrix} \cos\dfrac{\theta(t)}{2} & \sin\dfrac{\theta(t)}{2}e^{-i\phi(t)} \\ -\sin\dfrac{\theta(t)}{2}e^{i\phi(t)} & \cos\dfrac{\theta(t)}{2} \end{pmatrix}. \tag{2}$$

For an extremely slow variation of the external field, the spin-1/2 particle remains at the same instantaneous eigenstate, $|\psi_{+/-}(t)\rangle$, if it is prepared at $|\psi_{+/-}(0)\rangle$ initially. During this adiabatic propagation, only the dynamic and geometric phases are accumulated. With respect to the instantaneous eigenbasis, a unitary transformation is thus defined as $U_{\mathrm{ad}}(t) = |\psi_+(t)\rangle U_{\mathrm{ad};++}(t)\langle\psi_+(0)| + |\psi_-(t)\rangle U_{\mathrm{ad};--}(t)\langle\psi_-(0)|$ with $U_{\mathrm{ad};++}(t) = \exp[i\varphi_d(t) + i\gamma_+(t)]$ and $U_{\mathrm{ad};--}(t) = \exp[-i\varphi_d(t) + i\gamma_-(t)]$. Here $\varphi_d(t) = -(1/2)\int_0^t \Omega(\tau)\mathrm{d}\tau$ and $\gamma_\pm(t) = i\int_0^t \langle\psi_\pm(\tau)|\partial_\tau|\psi_\pm(\tau)\rangle \mathrm{d}\tau$ are the dynamic and geometric phases, respectively. In a matrix representation, this adiabatic unitary transformation is explicitly written as

$$U_{\mathrm{ad}}(t) = \begin{pmatrix} e^{i\varphi_d(t)+i\gamma_+(t)} & 0 \\ 0 & e^{-i\varphi_d(t)+i\gamma_-(t)} \end{pmatrix}. \tag{3}$$

In our experiment, we consider a special form of the amplitude evolution,

$$\Omega(t) = A\sin\left(\frac{2\pi t}{T}\right), \tag{4}$$

where the parameter T is the time of our quantum operation. The accumulated dynamic phases vanish, i.e., $\varphi_d(T) = 0$. After a global phase shift, the unitary transformation is simplified to

$$U_{\mathrm{ad}}(T) = \begin{pmatrix} 1 & 0 \\ 0 & e^{-i\Delta\gamma(T)} \end{pmatrix}, \tag{5}$$

with $\Delta\gamma(T) = \gamma_+(T) - \gamma_-(T)$. If the initial preparation and final measurement are performed in the reference basis of $\{|\uparrow\rangle, |\downarrow\rangle\}$, the combined unitary transformation is given by

$$U = S^+(T) U_{\mathrm{ad}}(T) S(0), \qquad (6)$$

which leads to an arbitrary single-qubit quantum gate [1]. This adiabatic construction can be straightforwardly extended to multi-qubit gates, which will be studied in the future.

2.2. STA protocol

In practice, the remaining non-adiabatic transition introduces an inevitable error for an adiabatic quantum gate. In the STA protocol, an additional counter-diabatic Hamiltonian is applied to cancel this non-adiabatic error [9–17]. A general time-dependent Hamiltonian $H_0(t)$ can be expanded in its instantaneous eigenbasis, giving $H_0(t) = \sum_n \epsilon_n(t)|\psi_n(t)\rangle\langle\psi_n(t)|$ with $\epsilon_n(t)$ the nth eigenenergy and $|\psi_n(t)\rangle$ the nth eigenstate. Accordingly, the counter-diabatic Hamiltonian $H_{\mathrm{cd}}(t)$ is formally written as [10]

$$H_{\mathrm{cd}}(t) = \mathrm{i}\hbar \sum_n [|\partial_t\psi_n(t)\rangle\langle\psi_n(t)| - \langle\psi_n(t)|\partial_t\psi_n(t)\rangle|\psi_n(t)\rangle\langle\psi_n(t)|], \qquad (7)$$

which suppresses the non-adiabatic transition for each eigenstate $|\psi_n(t)\rangle$. The quantum system driven $H(t) = H_0(t) + H_{\mathrm{cd}}(t)$ rigorously evolves along the instantaneous eigenstates of $H_0(t)$. The time propagator becomes exactly diagonal in the reference instantaneous eigenbasis, i.e.,

$$U_{\mathrm{STA}}(t) = \sum_n |\psi_n(t)\rangle U_{\mathrm{STA};nn}(t)\langle\psi_n(0)|. \qquad (8)$$

Each diagonal element of the time propagator is written as $U_{\mathrm{STA};nn}(t) = \exp\{\mathrm{i}[\varphi_{d;n}(t) + \gamma_n(t)]\}$ where $\varphi_{d;n}(t)$ and $\gamma_n(t)$ are accumulated dynamic and geometric phases of the nth reference adiabatic state. The adiabatic quantum gate introduced in equation (6) is thus changed to a STA quantum gate,

$$U = S^+(T) U_{\mathrm{STA}}(T) S(0), \qquad (9)$$

by replacing $U_{\mathrm{ad}}(T)$ with $U_{\mathrm{STA}}(T)$ and excluding the global phase. As the quantum operation time T is decreased, the error induced by relaxation and decoherence can be significantly reduced while the non-adiabatic error is fully suppressed in the ideal scenario. The STA protocol provides an alternative design of high-fidelity quantum gates [25].

For the spin-1/2 particle under the Hamiltonian in equation (1), the counter-diabatic Hamiltonian follows a similar form,

$$H_{\mathrm{cd}}(t) = \hbar B_{\mathrm{cd}}(t) \cdot \boldsymbol{\sigma}/2. \qquad (10)$$

Through a tedious but straightforward derivation from equation (7), the three elements of the counter-diabatic field $B_{\mathrm{cd}}(t)$ are explicitly given by

$$\begin{cases} B_{\mathrm{cd};x}(t) = -\dot{\theta}(t)\sin\phi(t) - \dot{\phi}(t)\sin\theta(t)\cos\theta(t)\cos\phi(t) \\ B_{\mathrm{cd};y}(t) = \dot{\theta}(t)\cos\phi(t) - \dot{\phi}(t)\sin\theta(t)\cos\theta(t)\sin\phi(t) \\ B_{\mathrm{cd};z}(t) = \dot{\phi}(t)\sin^2\theta(t). \end{cases} \qquad (11)$$

Equation (11) can be further organized into a cross product form as [10, 23, 24]

$$B_{\mathrm{cd}}(t) = \frac{1}{|B_0(t)|^2} B_0(t) \times \dot{B}_0(t), \qquad (12)$$

which is always orthogonal to the reference field $B_0(t)$. By applying the external field, $B(t) = B_0(t) + B_{\mathrm{cd}}(t)$, to a single-qubit, the STA gates will be testified experimentally in our Xmon qubit system.

2.3. DRAG correction

In many artificial systems, the influence of higher excited states cannot be fully ignored so that the two-level qubit has to be re-modeled as a multi-level anharmonic oscillator [1, 32]. For example, the Hamiltonian of a three-level anharmonic oscillator in the rotating frame is written as [24]

$$H(t) = \frac{\hbar}{2} B(t) \cdot S + \hbar\Delta_2|2\rangle\langle2|, \qquad (13)$$

where the operator vector S is given by

$$\begin{cases} S_x = \sum_{n=0}^1 \sqrt{n+1}\,(|n+1\rangle\langle n| + |n\rangle\langle n+1|) \\ S_y = \sum_{n=0}^1 \sqrt{n+1}\,(\mathrm{i}|n+1\rangle\langle n| - \mathrm{i}|n\rangle\langle n+1|) \\ S_z = \sum_{n=0}^2 (1-2n)|n\rangle\langle n| \end{cases} \qquad (14)$$

and Δ_2 is an anharmonic parameter. In the STA protocol, the external field is given by $B(t) = B_0(t) + B_{cd}(t)$. A technical treatment is to apply the derivative removal by adiabatic gates (DRAG) method, which decouples the interaction between the lowest two levels (qubit) and higher excited states [24, 28–31]. With the increment of another field, $B_d(t) = (B_{d;x}(t), B_{d;y}(t), B_{d;z}(t))$, the total external field is changed to $B_{tot}(t) = B(t) + B_d(t)$ and the total Hamiltonian in equation (13) is modified to be $H'(t) = (\hbar/2)B_{tot}(t) \cdot S + \hbar\Delta_2|2\rangle\langle2|$. In addition, we introduce the DRAG frame ($\mathcal{D}$-frame), in which the total Hamiltonian is transformed into

$$H_{\mathcal{D}}(t) = \mathcal{D}^+(t)H'(t)\mathcal{D}(t) + i\dot{\mathcal{D}}^+(t)\mathcal{D}(t) \tag{15}$$

where $\mathcal{D}(t)$ is a unitary operator. The density matrix in the $\mathcal{D}$-frame is given by $\rho_{\mathcal{D}}(t) = \mathcal{D}(t)\rho(t)\mathcal{D}^+(t)$. With a delicate design of $B_{tot}(t)$ and $\mathcal{D}(t)$, the transformed Hamiltonian $H_{\mathcal{D}}(t)$ is factorized into

$$H_{\mathcal{D}}(t) = \left[\varepsilon(t) + \frac{\hbar}{2}B(t) \cdot \boldsymbol{\sigma}\right] \oplus \varepsilon_2(t)|2\rangle\langle2|, \tag{16}$$

where $\varepsilon(t)$ and $\varepsilon_2(t)$ are two shifted energies [24, 29]. The qubit subspace of $\{|0\rangle, |1\rangle\}$ is decoupled with the second excited state $|2\rangle$. To avoid an artifact of the $\mathcal{D}$-frame, we would expect an requirement of

$$\mathcal{D}(t = 0) = 1 \quad \text{and} \quad \mathcal{D}(t = T) = 1, \tag{17}$$

so that the density matrices at the initial and final moments of the quantum operation are unaffected, i.e., $\rho_{\mathcal{D}}(0) = \rho(0)$ and $\rho_{\mathcal{D}}(T) = \rho(T)$. In the DRAG method, $B_{tot}(t)$ and $\mathcal{D}(t)$ are evaluated by a perturbation approach with the assumption of a large anharmoncity, i.e., $|\Delta_2| \gg |B(t)|$. On the first order correction, the DRAG field $B_d(t)$ is explicitly given by [24, 29]

$$\begin{cases} B_{d;x}(t) = \dfrac{1}{2\Delta_2}[\dot{B}_y(t) - B_z(t)B_x(t)] \\[2mm] B_{d;y}(t) = -\dfrac{1}{2\Delta_2}[\dot{B}_x(t) + B_z(t)B_y(t)] \\[2mm] B_{d;z}(t) = 0, \end{cases} \tag{18}$$

under a presumption of $B_{d;z}(t) = 0$. In our experiment, the Xmon qubit is driven by the total external field, $B_{tot}(t) = B_0(t) + B_{cd}(t) + B_d(t)$, under the STA protocol and with the DRAG correction.
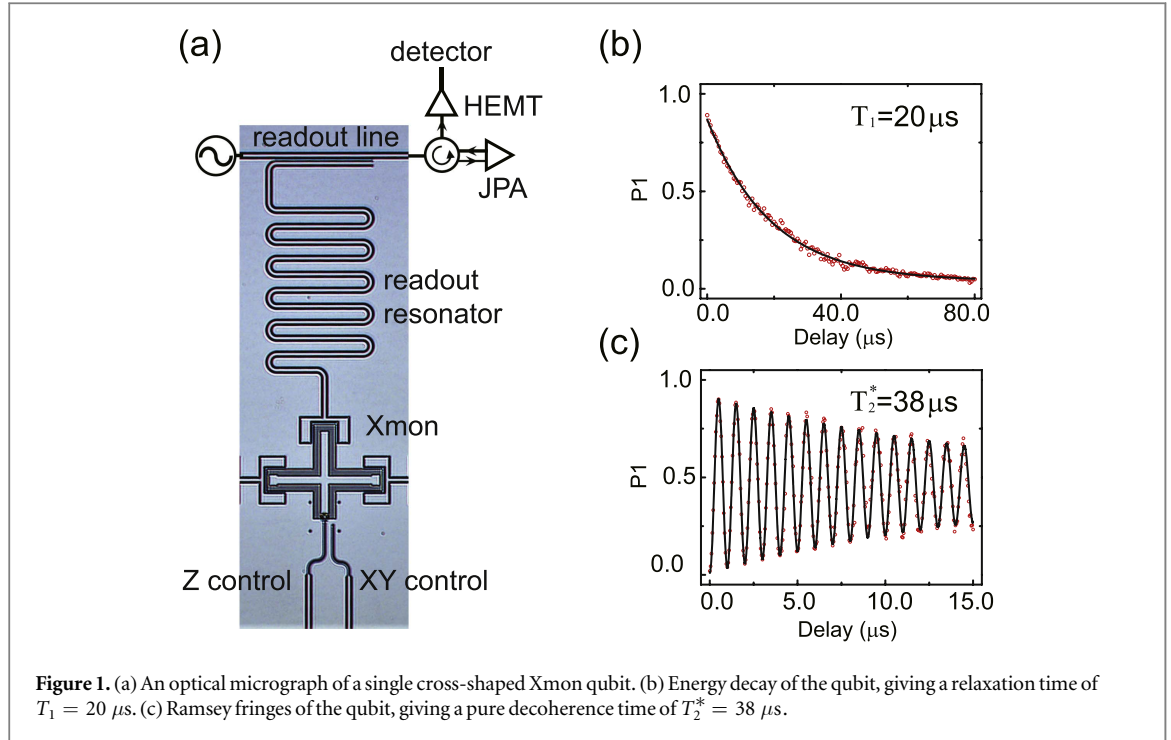
3. Experimental setup

A cross-shaped transmon (or called Xmon) qubit [6, 32, 33] is applied in this experiment. The Xmon qubit sample is fabricated on a silicon substrate. After initially cleaned in buffered hydrofluoric acid to remove the native oxide, the substrate is immediately loaded into a high vacuum electron beam evaporator, followed by a deposition of an aluminum (Al) film. The superconducting resonators and control lines are patterned using photolithography in a wafer stepper and etched with BCl_3/Cl_2 in an inductively coupled plasma dry etcher. The superconducting Josephson junctions are patterned with an electron beam lithography and developed with Al double-angle evaporation. An additional 'bandage' DC electrical contact is fabricated to reduce the capacitive loss [34].

Figure 1(a) displays an optical micrograph of a single Xmon qubit. Four arms of the cross are connected to different elements for separate functions of coupling, control and readout. At the bottom of the cross, a flux current (Z control) line biases the qubit at a resonance frequency of $\omega_{10}/2\pi = 4.85$ GHz, which is the energy difference between the ground ($|0\rangle$) and excited ($|1\rangle$) states of the qubit. The qubit nonlinearity is $\Delta_2/2\pi = -253$ MHz. Another *XY* control line provides a microwave drive signal to the qubit to manipulate the qubit state [6, 32, 33]. The top arm of the cross is coupled to a readout resonator whose bare frequency is $\omega_r/2\pi = 6.56$ GHz. By sending a microwave signal through the readout line, we can detect the qubit state information from the dispersive interaction between the qubit and readout resonator. The readout signal goes through a series of circulators, being reflected from a Josephson parametric amplifier [35, 36] and further amplified by a high electron mobility transistor for a high-fidelity measurement. By heralding the ground state [37], the readout fidelity for the ground state $|0\rangle$ and excited state $|1\rangle$ are 99.8% and 95.1%, respectively. With the qubit biased at a sweet point here, the coherence is characterized by a relaxation time, $T_1 = 20\ \mu$s, and a pure decoherence time, $T_2^* = 38\ \mu$s (see figures 1(b) and (c)). Our current sample is designed as a linear array with six qubits. All the qubits have comparable values of T_1 and T_2^*. The qubit chip is mounted in a sample box and cooled in a dilution refrigerator whose base temperature is $\sim$10 mK.

4. Results

In this section, we present our experimental realization of various single-qubit STA quantum gates.

Figure 1. (a) An optical micrograph of a single cross-shaped Xmon qubit. (b) Energy decay of the qubit, giving a relaxation time of $T_1 = 20~\mu s$. (c) Ramsey fringes of the qubit, giving a pure decoherence time of $T_2^* = 38~\mu s$.

4.1. X_π and $X_{\pi/2}$ rotations

The unitary matrices representing the π and $\pi/2$ rotations about the X-axis (X_π and $X_{\pi/2}$ rotations) are explicitly written as [1]

$$U_{X_\pi} = \begin{pmatrix} 0 & -i \\ -i & 0 \end{pmatrix} \quad \text{and} \quad U_{X_{\pi/2}} = \frac{\sqrt{2}}{2}\begin{pmatrix} 1 & -i \\ -i & 1 \end{pmatrix}. \tag{19}$$

To design the X_π rotation, the reference 'adiabatic' field $B_0(t)$ is specified as

$$\begin{cases} B_{0;x}(t) = 0 \\ B_{0;y}(t) = -\Omega(t)\sin\theta(t) \\ B_{0;z}(t) = \Omega(t)\cos\theta(t). \end{cases} \tag{20}$$
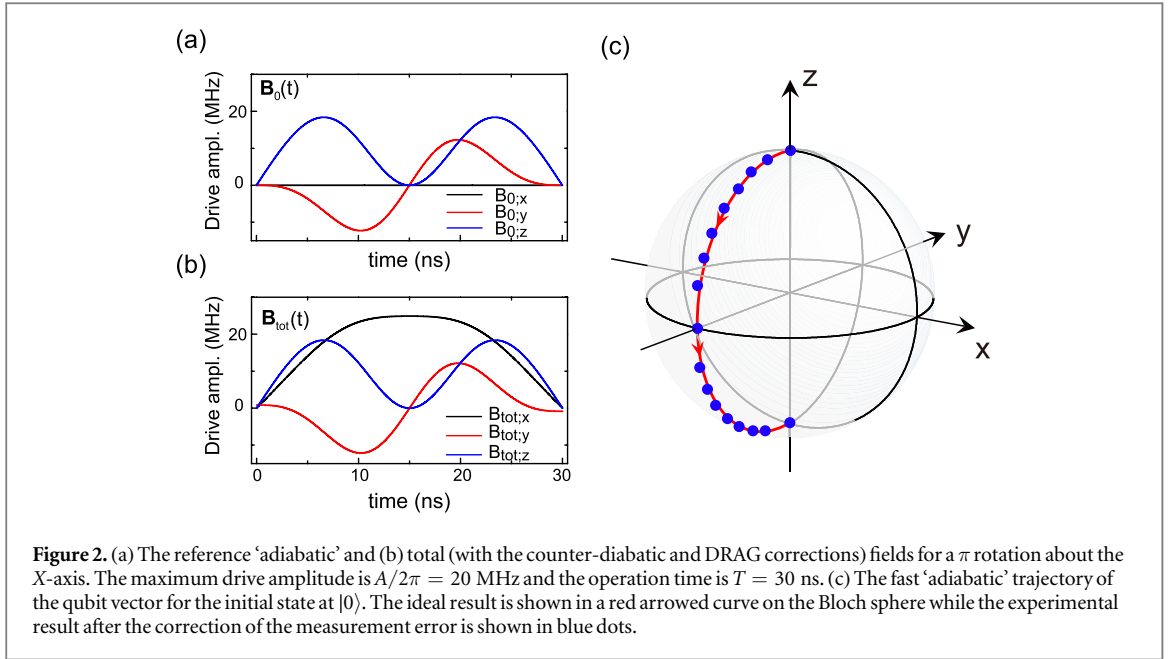
The drive amplitude, polar and azimuthal angles are $\Omega(t) = A\sin(2\pi t/T)$, $\theta(t) = (\pi/2)[1 - \cos(\pi t/T)]$, and $\phi(t) = -\pi/2$, respectively. In our experiment, we set the pulse length (operation time) at $T = 30$ ns and the maximum drive amplitude at $A/2\pi = 20$ MHz. The same two parameters will be used in other STA gates. The pulse length is comparable to the typical value of a truncated Gaussian pulse. In principle, these two parameters can be modified independently under the STA protocol. The counter-diabatic field $B_{cd}(t)$ and the DRAG field $B_d(t)$ are calculated using equations (11) and (18). Due to the limitation of space, we will not present the analytical forms of $B_{cd}(t)$ and $B_d(t)$. In figures 2(a) and (b), we plot the x-, y- and z-components of the reference field $B_0(t)$ and the total field $B_{tot}(t) = B_0(t) + B_{cd}(t) + B_d(t)$. As a comparison, the major difference between the two fields appears in their x-components. With the condition of $|A| \ll |\Delta_2|$, the DRAG correction is a minor effect. Notice that if the amplitude of $B_0(t)$ is gradually decreased to zero, the dominant counter-diabatic field $B_{cd}(t)$ recovers the standard X_π-pulse along the x-direction. Thus, other gate schemes can in principle be mapped onto their counterparts in the STA protocol. For an initial preparation at the spin-up state ($|\uparrow\rangle = |0\rangle$), the fast 'adiabatic' trajectory of the qubit is shown in figure 2(c). In an ideal scenario, the qubit vector evolves from the north to south pole along $270°$-longitude of the Bloch sphere, and the final qubit state is the spin-down state ($|\downarrow\rangle = |1\rangle$). Figure 2(c) shows that this trajectory can be excellently generated under the STA control field $B_{tot}(t)$ [24].

With the consideration of the errors in state preparation, STA operation and readout, the output state is obtained through a map of the input state [1], i.e.,

$$\varepsilon: \rho \mapsto \varepsilon(\rho) = \sum_{i=1}^{4} E_i \rho E_i^+, \tag{21}$$

with ρ the initial density matrix of the qubit. Each linear operators $E_{i=1,\cdots,4}$ can be expanded over a fixed set of operators, $\{\tilde{E}_m = I, \sigma_x, \sigma_y, \sigma_z\}$, giving $E_i = \sum_m e_{im}\tilde{E}_m$. The output density matrix is rewritten as

Figure 2. (a) The reference 'adiabatic' and (b) total (with the counter-diabatic and DRAG corrections) fields for a π rotation about the X-axis. The maximum drive amplitude is $A/2\pi = 20$ MHz and the operation time is $T = 30$ ns. (c) The fast 'adiabatic' trajectory of the qubit vector for the initial state at $|0\rangle$. The ideal result is shown in a red arrowed curve on the Bloch sphere while the experimental result after the correction of the measurement error is shown in blue dots.

$$\varepsilon(\rho) = \sum_{mn} \chi_{mn} \tilde{E}_m \rho \tilde{E}_n^+ \qquad (22)$$

with $\chi_{mn} = \sum_i e_{im} e_{in}^*$. The χ matrix thus completely characterizes the behavior of a specific gate. To experimentally determine the χ matrix, we perform the QPT by selecting 6 different initial states, $\{|0\rangle, |1\rangle, (|0\rangle \pm |1\rangle)/\sqrt{2}$, $(|0\rangle \pm i|1\rangle)/\sqrt{2}\}$ [1, 38, 39]. Each input state is driven by $B_{tot}(t)$ and the output state is measured by the quantum state tomography method. The χ matrix is then numerically calculated by solving equation (22). For the STA X_π-gate, the experimental result of the $\chi(X_\pi)$ matrix is plotted in figures 3(a) and (b). Consistent with the theoretical prediction of an ideal X_π-gate, the dominant element of the $\chi(X_\pi)$ matrix is the operator of σ_x. To quantify the fidelity of the whole quantum process, we calculate the process fidelity using [1]

$$F_P = \text{Tr}\{\chi\chi_{\text{ideal}}\}. \qquad (23)$$

The experimental result is $F_P(X_\pi) = 95.21\%$. To exclude the errors in state preparation and readout, we perform an interleaved randomized benchmarking measurement (see section 4.4), which gives the gate fidelity of the STA X_π rotation at $F_g(X_\pi) = 99.82\%$. This number is very close to the current highest fidelity of a Xmon qubit [6], and the 0.1% deviation could be improved by the future optimization of our system. On the other hand, if the operation time is increased to $T = 500$ ns, the counter-diabatic field becomes nearly negligible and the process fidelity of the adiabatic X_π-gate is decreased to $F_P(X_\pi) = 92.15\%$ due to the accumulation of the dissipation-induced error.

To design the $X_{\pi/2}$ rotation, we take the same reference 'adiabatic' field $B_0(t)$ except for that the azimuthal angle is changed to $\theta(t) = (\pi/4)[1 - \cos(\pi t/T)]$. The counter-diabatic and DRAG fields, $B_{cd}(t)$ and $B_d(t)$, are analytically calculated accordingly. After the QPT measurement, the experimentally reconstructed $\chi(X_{\pi/2})$ matrix is plotted in figures 3(c) and (d), agreeing excellently with the theoretical prediction of an ideal $X_{\pi/2}$ gate. As compared to the $\chi(X_\pi)$ matrix, the $\chi(X_{\pi/2})$ matrix includes auto and cross correlations between the operators of I and σ_x. The experimental measurement shows that the process and gate fidelities of our STA $X_{\pi/2}$ rotation are $F_P(X_{\pi/2}) = 95.03\%$ and $F_g(X_{\pi/2}) = 99.81\%$.
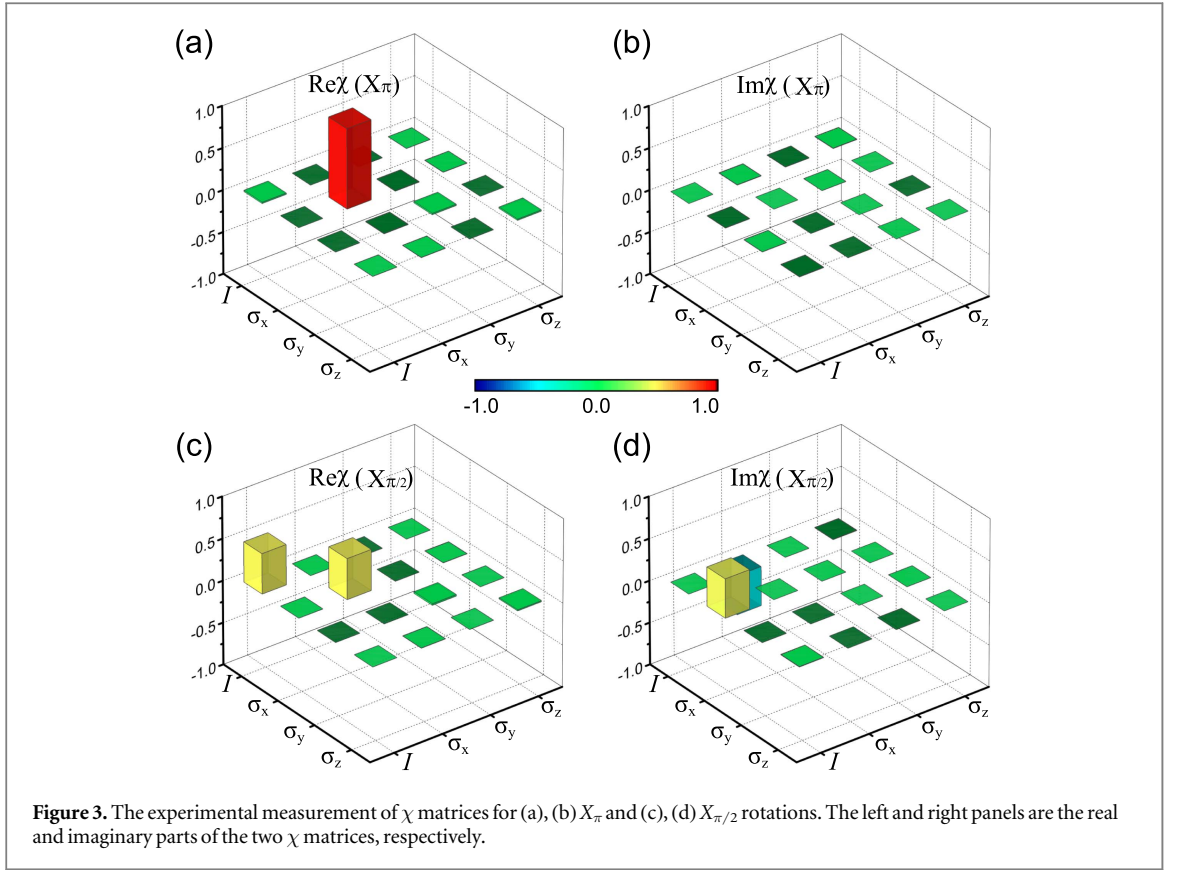
4.2. Z_π and $Z_{\pi/2}$ rotations

The second group of STA quantum gates we inspect are the π and $\pi/2$ rotations about Z-axis. The corresponding unitary matrices are [1]

$$U_{Z_\pi} = \begin{pmatrix} -i & 0 \\ 0 & i \end{pmatrix}, \quad \text{and} \quad U_{Z_{\pi/2}} = \begin{pmatrix} e^{-i\pi/4} & 0 \\ 0 & e^{i\pi/4} \end{pmatrix}. \qquad (24)$$

To design these two gates, the reference 'adiabatic' field $B_0(t)$ is specified as

$$\begin{cases} B_{0;x}(t) = \Omega(t)\cos\phi(t) \\ B_{0;y}(t) = \Omega(t)\sin\phi(t) \\ B_{0;z}(t) = 0, \end{cases} \qquad (25)$$

Figure 3. The experimental measurement of χ matrices for (a), (b) X_π and (c), (d) $X_{\pi/2}$ rotations. The left and right panels are the real and imaginary parts of the two χ matrices, respectively.

where the drive amplitude is $\Omega(t) = A \sin(2\pi t/T)$ and the polar angle is $\theta(t) = \pi/2$. The azimuthal angles for Z_π and $Z_{\pi/2}$ rotations are $\phi(t) = (\pi/2)[1 - \cos(\pi t/T)]$ and $\phi(t) = (\pi/4)[1 - \cos(\pi t/T)]$, respectively. The control parameters, A and T, are the same as those in the X-rotation gates. The counter-diabatic and DRAG fields, $B_{cd}(t)$ and $B_d(t)$, are also analytically calculated for the experimental generation. The QPT measurements of $\chi(Z_\pi)$ and $\chi(Z_{\pi/2})$ matrices are presented in figures 4(a)–(d), also agreeing excellently with the results in an ideal scenario. The process fidelities of these two STA gates are $F_P(Z_\pi) = 95.23\%$ and $F_P(Z_{\pi/2}) = 95.20\%$. After excluding errors in state preparation and readout, the gates fidelities are $F_g(Z_\pi) = 99.89\%$ and $F_g(Z_{\pi/2}) = 99.87\%$.

4.3. Hadamard gate

An arbitrary single-qubit quantum gate can be realized by a combination of sequential rotations about X-, Y- and Z-axes. For example, the Hadamard gate can be generated by $\pi/2$ rotation about the Y-axis followed by π rotation about the X-axis [1], i.e.,
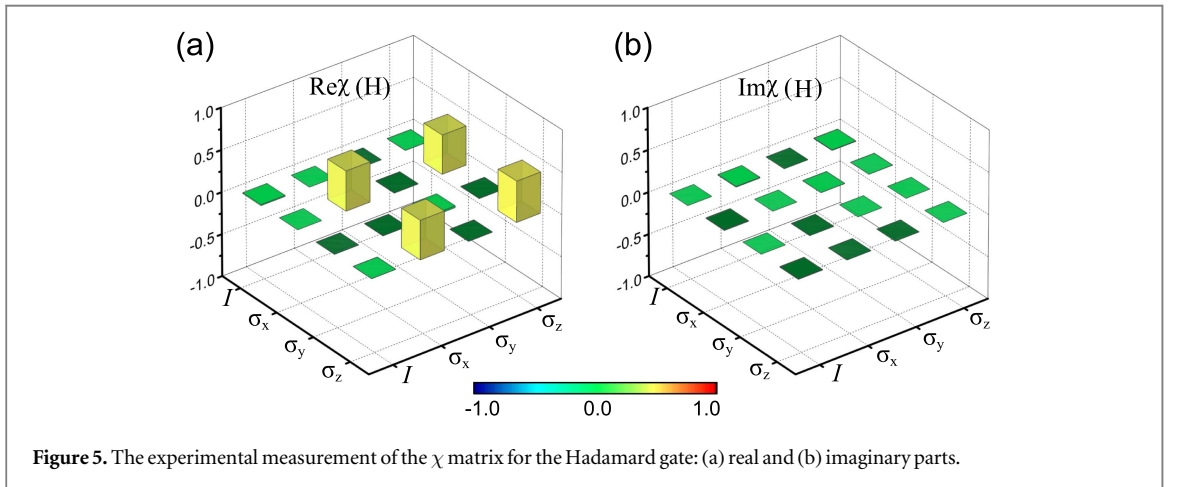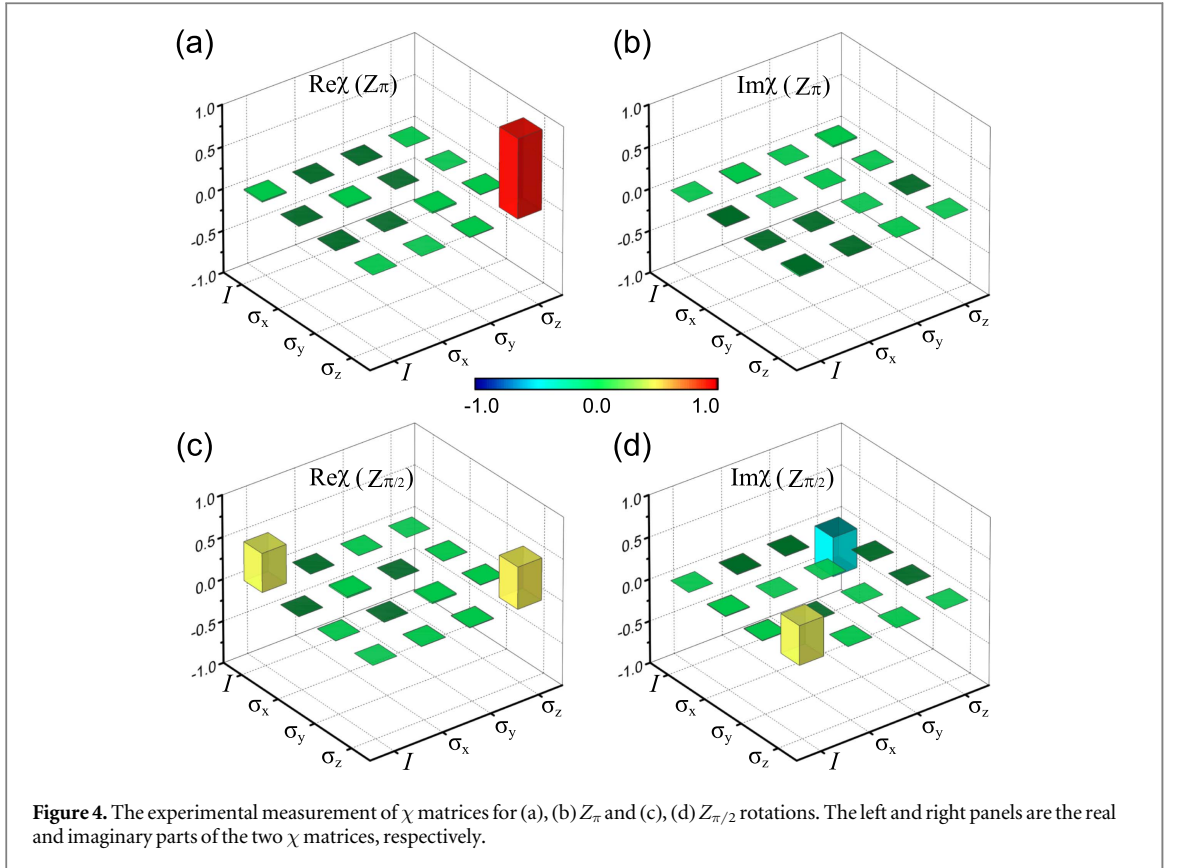
$$U_H = U_{X_\pi} U_{Y_{\pi/2}} = \frac{\sqrt{2}}{2} \begin{pmatrix} 1 & 1 \\ 1 & -1 \end{pmatrix}. \tag{26}$$

In the STA protocol, the Hadamard gate can be realized by a one-step operation, which reduces the errors accumulated through multiple steps. Our reference 'adiabatic' field $B_0(t)$ is designed as

$$\begin{cases} B_{0;x}(t) = \dfrac{\sqrt{2}}{2}\Omega(t)\cos\varphi(t) \\[2mm] B_{0;y}(t) = \Omega(t)\sin\varphi(t) \\[2mm] B_{0;z}(t) = -\dfrac{\sqrt{2}}{2}\Omega(t)\cos\varphi(t) \end{cases} \tag{27}$$

with $\Omega(t) = A \sin(2\pi t/T)$ and $\varphi(t) = (\pi/2)[1 - \cos(\pi t/T)]$. After including counter-diabatic field $B_{cd}(t)$ and the DRAG field $B_d(t)$, we perform the same QPT measurement as above. The experimentally reconstructed $\chi(H)$ matrix is displayed in figures 5(a) and (b). The process fidelity is $F_P(H) = 94.93\%$ while the gate fidelity with the errors in state preparation and readout excluded is $F_g(H) = 99.81\%$.
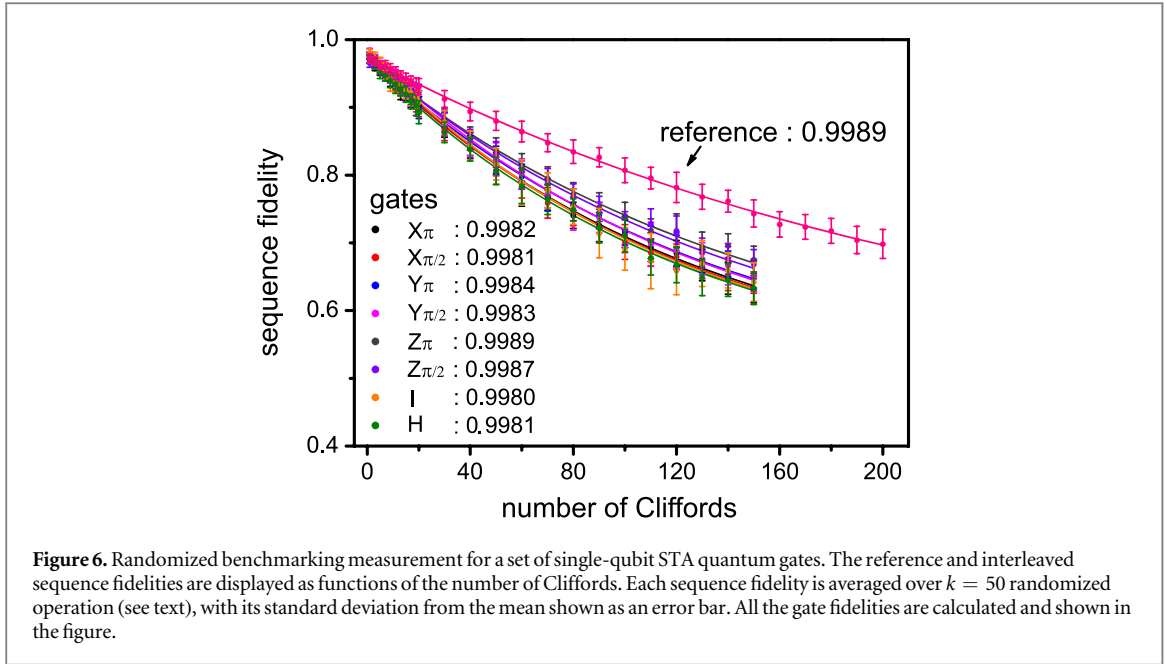
Figure 4. The experimental measurement of χ matrices for (a), (b) Z_π and (c), (d) $Z_{\pi/2}$ rotations. The left and right panels are the real and imaginary parts of the two χ matrices, respectively.

Figure 5. The experimental measurement of the χ matrix for the Hadamard gate: (a) real and (b) imaginary parts.

4.4. Interleaved randomized benchmarking measurement

In the QPT measurement, the errors of state preparation and readout are mixed with the error of a quantum gate operation. To extract the gate fidelity, we perform the Clifford-based randomized benchmarking measurement [6, 40–43]. For a single-qubit, the Clifford group consists of 24 rotations preserving the octahedron in the Bloch sphere. In principle, each Clifford operator can be realized by a combination from the elements of $\{I, X_\pi, X_{\pm\pi/2}, Y_\pi, Y_{\pm\pi/2}\}$. The qubit is initially prepared at the spin-up state ($|\uparrow\rangle = |0\rangle$), and then driven by a sequence of m randomly selected Clifford gates. The combined operation is described by a unitary matrix, $U_C = \prod_{i=1}^{m} U_i$. Since the Clifford group is a closed set, U_C is always a Clifford operator. Subsequently, the $(m + 1)$th step is the reversed step of U_C and the total quantum operation is written as

$$U_{\text{tot}} = U_C^+ \prod_{i=1}^{m} U_i. \tag{28}$$

The remaining population $P_0(t_f)$ of the initial state is measured afterwards. After repeating the above random operation sequence k (=50 in our experiment) times, we calculate the average result of $P_0(t_f)$, which represents a

Figure 6. Randomized benchmarking measurement for a set of single-qubit STA quantum gates. The reference and interleaved sequence fidelities are displayed as functions of the number of Cliffords. Each sequence fidelity is averaged over $k = 50$ randomized operation (see text), with its standard deviation from the mean shown as an error bar. All the gate fidelities are calculated and shown in the figure.

sequence fidelity, $F_{\text{seq}}(m)$. As shown in figure 6, this sequence fidelity can be well fitted by a power-law decaying function [41],

$$F_{\text{seq}} = A_0 p^m + B_0, \tag{29}$$

where A_0 and B_0 absorbs the errors in state preparation and readout, and p is a depolarizing parameter. The average error over the randomized Clifford gates is given by [41]

$$r = \frac{d-1}{d}(1-p), \tag{30}$$

where $d = 2^N$ is the dimension of the Hilbert space for an array of N qubits. In our experiment, the value of the average error is $r = 0.0011$, or equivalently the fidelity of a randomized Clifford gate is 99.89%, which serves as a reference for our next interleaved operation (see figure 6).

To extract the fidelity of a specific gate U_g, we make an interleaved operation [41]. At each step, the qubit is driven by a combination of a randomly select Clifford operator followed U_g. With the product operator, $U'_C = \prod_{i=1}^{m} (U_g U_i)$, and the $(m+1)$th operator of $(U'_C)^+$, the total quantum operation is described by $U'_{\text{tot}} = (U'_C)^+ \prod_{i=1}^{m} (U_g U_i)$ [6, 41]. Similarly, we measure the sequence fidelity $F'_{\text{seq}}(m)$. As shown by the examples in figure 6, $F'_{\text{seq}}(m)$ can also be well fitted by equation (29) with a new depolarizing parameter p'. Here p' can be considered as a product of the average number p of a randomized Clifford operator and the intrinsic number p_g of the specific gate U_g, i.e., $p_g = p'/p$. Substituting p_g into equation (30), we obtain the intrinsic error r_g and the gate fidelity of U_g is given by

$$F_g = 1 - \frac{d-1}{d}\left(1 - \frac{p'}{p}\right). \tag{31}$$

In figure 6, we list the results of 8 example STA gates, and all the values of F_g are equal or greater than 99.8%. In the STA protocol, the fidelity of the Hadamard gate ($F_g(H) = 99.81\%$) is higher than the product of the fidelities of the $Y_{\pi/2}$ and X_π gates ($F_g(X_\pi)F_g(Y_{\pi/2}) = 99.65\%$). Thus, our one-step STA gate can efficiently reduce the error accumulation in a combined operation of multiple gates.

5. Summary

In this paper, we propose a scheme of building a universal quantum gate using a 'STA' trajectory, which shares the same spirit as in [25] but with a different design. This scheme is successfully implemented in a high-quality superconducting Xmon qubit, and various single-qubit STA quantum gates are created through a precise microwave control. As demonstrated by the examples of rotations about X- and Z-axes and the Hadamard gate, we have achieved high process and gate fidelities ($F_p > 94.9\%$ and $F_g \geqslant 99.8\%$), which are very close to the state-of-the-art values ($F_g \geqslant 99.91\%$) in the superconducting Xmon qubit system. In principle, the STA quantum gates allow a large flexibility in the control parameters, such as the pulse amplitude, operation time and

pulse shape. Although this paper is focused on single-qubit gates, the STA scheme can be extended to a multi-qubit system [6, 25]. The improvement and extension of our STA quantum gates will be addressed in the near future.

Acknowledgments

References

[1] Nielsen M A and Chuang I L 2000 *Quantum Computation and Quantum Information* (Cambridge: Cambridge University Press)
[2] Ladd T D, Jelezko F, Laflamme R, Nakamura Y, Monroe C and O'Brien J L 2010 *Nature* **464** 45–53
[3] Ryan C, Laforest M and Laflamme R 2009 *New J. Phys.* **11** 013034
[4] Lu D *et al* 2017 *npj Quantum Inf.* **3** 45
[5] Benhelm J, Kirchmair G, Roos C F and Blatt R 2008 *Nat. Phys.* **4** 463–6
[6] Barends R *et al* 2014 *Nature* **508** 500–3
[7] Sjöqvist E 2008 *Physics* **1** 35
[8] Zhu S L and Zanardi P 2005 *Phys. Rev.* A **72** 020301
[9] Demirplak M and Rice S A 2003 *J. Phys. Chem.* A **107** 9937–45
[10] Berry M 2009 *J. Phys. A: Math. Theor.* **42** 365303
[11] Chen X, Lizuain I, Ruschhaupt A, Guéry-Odelin D and Muga J 2010 *Phys. Rev. Lett.* **105** 123003
[12] Masuda S and Nakamura K 2010 *Proc. R. Soc.* A **466** 1135–54
[13] Torrontegui E, Ibáñez S, Martínez-Garaot S, Modugno M, del Campo A, Guéry-Odelin D, Ruschhaupt A, Chen X and Muga J G 2013 *Adv. At. Mol. Opt. Phys.* **62** 117–69
[14] del Campo A, Rams M M and Zurek W H 2012 *Phys. Rev. Lett.* **109** 115703
[15] del Campo A 2013 *Phys. Rev. Lett.* **111** 100502
[16] Zhang J, Kyaw T H, Tong D M, Sjöqvist E and Kwek L C 2015 *Sci. Rep.* **5** 18414
[17] Santos A C and Sarandy M S 2015 *Sci. Rep.* **5** 15775
[18] Bason M G, Viteau M, Malossi N, Huillery P, Arimondo E, Ciampini D, Fazio R, Giovannetti V, Mannella R and Morsch O 2012 *Nat. Phys.* **8** 147–52
[19] Zhang J F *et al* 2013 *Phys. Rev. Lett.* **110** 240501
[20] An S M, Lv D S, del Campo A and Kim K 2016 *Nat. Commun.* **7** 12999
[21] Du Y X, Liang Z T, Li Y C, Yue X X, Lv Q X, Huang W, Chen X, Yan H and Zhu S L 2016 *Nat. Commun.* **7** 12479
[22] Zhou B B, Baksic A, Ribeiro H, Yale C G, Heremans F J, Jerger P C, Auer A, Burkard G, Clerk A A and Awschalom D D 2017 *Nat. Phys.* **13** 330–4
[23] Zhang Z X, Wang T H, Xiang L, Yao J D, Wu J L and Yin Y 2017 *Phys. Rev.* A **95** 042345
[24] Wang T H, Zhang Z X, Xiang L, Gong Z H, Wu J L and Yin Y 2018 *Sci. China Phys. Mech.* **61** 047411
[25] Liang Z T, Yue X X, Lv Q X, Du Y X, Huang W, Yan H and Zhu S L 2016 *Phys. Rev.* A **93** 040305
[26] Masuda S, Tan K Y and Nakahara M 2018 *Phys. Rev.* B **97** 045418
[27] Vepsäläinen A, Danilin S and Paraoanu G S 2018 *Quantum Sci. Technol.* **3** 024006
[28] Motzoi F, Gambetta J M, Rebentrost P and Wilhelm F K 2009 *Phys. Rev. Lett.* **103** 110501
[29] Gambetta J M, Motzoi F, Merkel S T and Wilhelm F K 2011 *Phys. Rev.* A **83** 012308
[30] Lucero E *et al* 2010 *Phys. Rev.* A **82** 042339
[31] Chow J M, DiCarlo L, Gambetta J M, Motzoi F, Frunzio L, Girvin S M and Schoelkopf R J 2010 *Phys. Rev.* A **82** 040305
[32] Barends R *et al* 2013 *Phys. Rev. Lett.* **111** 080502
[33] Kelly J *et al* 2015 *Nature* **519** 66–9
[34] Dunsworth A *et al* 2017 *Appl. Phys. Lett.* **111** 022601
[35] Roy T, Kundu S, Chand M, Vadiraj A M, Ranadive A, Nehra N, Patankar M P, Aumentado J, Clerk A A and Vijay R 2015 *Appl. Phys. Lett.* **107** 262601
[36] Yuan X, Liu K, Xu Y, Wang W, Ma Y W, Zhang F, Yan Z P, Vijay R, Sun L Y and Ma X F 2016 *Phys. Rev. Lett.* **117** 010502
[37] Johnson J E, Macklin C, Slichter D H, Vijay R, Weingarten E B, Clarke J and Siddiqi I 2012 *Phys. Rev. Lett.* **109** 050506
[38] Bialczak R C *et al* 2010 *Nat. Phys.* **6** 409–13
[39] Yamamoto T *et al* 2010 *Phys. Rev.* B **82** 184515
[40] Knill E, Leibfried D, Reichle R, Britton J, Blakestad R B, Jost J D, Ozeri R, Seidelin S and Wineland D J 2008 *Phys. Rev.* A **77** 012307
[41] Magesan E *et al* 2012 *Phys. Rev. Lett.* **109** 080505
[42] Chow J M, Gambetta J M, Tornberg L, Koch J, Bishop L S, Houck A A, Johnson B R, Frunzio L, Girvin S M and Schoelkopf R J 2009 *Phys. Rev. Lett.* **102** 090502
[43] Sheldon S, Bishop L S, Magesan E, Filipp S, Chow J M and Gambetta J M 2016 *Phys. Rev.* A **93** 012301